Chemistry & Biology, Vol. 10, 1255–1266, December, 2003, ©2003 Elsevier Science Ltd. All rights reserved. DOI 10.1016/j.chembiol.2003.11.010

GSK-3-Selective Inhibitors Derived from Tyrian Purple Indirubins

Laurent Meijer,[1,2,*] Alexios-Leandros Skaltsounis,[4] Prokopios Magiatis,[4] Panagiotis Polychronopoulos,[4] Marie Knockaert,[1] Maryse Leost,[1] Xiaozhou P. Ryan,[2] Claudia Alin Vonica,[3] Ali Brivanlou,[3] Rana Dajani,[6] Claudia Crovace,[5] Cataldo Tarricone,[5] Andrea Musacchio,[5] S. Mark Roe,[6] Laurence Pearl,[6] and Paul Greengard[2]

[1]C.N.R.S.
Cell Cycle Group
Station Biologique, B.P. 74
29682 Roscoff cedex
Bretagne
France

[2]Laboratory of Molecular & Cellular Neuroscience
[3]Laboratory of Molecular Embryology
The Rockefeller University
1230 York Avenue
New York, New York 10021

[4]Division of Pharmacognosy and Natural Products Chemistry
Department of Pharmacy
University of Athens
Panepistimiopolis Zografou
GR-15771 Athens
Greece

[5]Structural Biology Unit
Department of Experimental Oncology
European Institute of Oncology
Via Ripamonti 435
20141 Milano
Italy

[6]Centre for Structural Biology
Institute of Cancer Research
Chester Beatty Laboratories
237 Fulham Road
London SW3 6JB
United Kingdom

Summary

Gastropod mollusks have been used for over 2500 years to produce the "Tyrian purple" dye made famous by the Phoenicians. This dye is constituted of mixed bromine-substituted indigo and indirubin isomers. Among these, the new natural product 6-bromoindirubin and its synthetic, cell-permeable derivative, 6-bromoindirubin-3′-oxime (BIO), display remarkable selective inhibition of glycogen synthase kinase-3 (GSK-3). Cocrystal structure of GSK-3β/BIO and CDK5/p25/indirubin-3′-oxime were resolved, providing a detailed view of indirubins' interactions within the ATP binding pocket of these kinases. BIO but not 1-methyl-BIO, its kinase inactive analog, also inhibited the phosphorylation on Tyr276/216, a GSK-3α/β activation site. BIO but not 1-methyl-BIO reduced β-catenin phosphorylation on a GSK-3-specific site in cellular models. BIO but not 1-methyl-BIO closely mimicked Wnt signaling in *Xenopus* embryos. 6-bromoindirubins thus provide a new scaffold for the development of selective and potent pharmacological inhibitors of GSK-3.

*Correspondence: meijer@sb-roscoff.fr

Introduction

In mammals, different genes encode two closely related glycogen synthase kinase-3 (GSK-3) enzymes, GSK-3α and GSK-3β. The discovery of GSK-3 functions in Wnt signal-transducing pathways, insulin action, apoptosis, and circadian rhythm, the deciphering of unique regulation mechanisms of GSK-3 (inhibitory phosphorylation on Ser9, priming of substrate by phosphorylation by another kinase), the determination of the crystal structure of human GSK-3β, and the clear implication of GSK-3 in various human diseases (diabetes, Alzheimer's disease, cancers) have all recently contributed to a renewed interest in this kinase (for reviews see [1–5]. Growing evidence supports the view that GSK-3β activation [6, 7] and nuclear translocation [8] are a prerequisite for neuronal apoptosis. The data stem from cell culture experiments in which apoptosis induced by various agents can be prevented in several ways, leading to GSK-3 inactivation: (1) overexpression of FRAT1, a negative regulator of GSK-3, confers resistance of PC12 cells to apoptosis [9, 10]; (2) pharmacological inhibitors of GSK-3 prevent apoptosis in PC12 cells [10–12], human SH-SY5Y neuroblastoma cells [13, 14], and a Huntington disease cell model [15]; (3) activation of Wnt signaling (and therefore GSK-3 inhibition) prevents c-Myc-induced apoptosis in Rat-1 cells [16]; (4) expression of a kinase-deficient GSK-3β reduces cell death induced by Akt inhibition [9]; (5) FGF (which activates Akt and thus inhibits GSK-3) reduces cell death induced by glutamate [17], while overexpression of GSK-3β increases cell death; and (6) inhibition of GSK-3 by Ser9 phosphorylation by PKA is associated with neuronal survival [18]. In addition to these in vitro data, two animal models reinforce the link between GSK-3 activation and apoptosis: (1) conditional transgenic mice overexpressing GSK-3 in brain during adulthood show signs of neuronal stress and apoptosis [19], and (2) expression of *shaggy*, the *Drosophila* homolog of GSK-3β, enhances the neurodegeneration induced by expression of human Tau in flies, while expression of a loss-of-function mutant of *shaggy* prevents this neurodegeneration [20].

Only a very limited number of pharmacological inhibitors of GSK-3 are available [21], lithium being the most frequently used [22] despite its effects being in the 10–20 mM range and its demonstrated effect on inositol phosphatases [23]. Recently, we noted that several pharmacological inhibitors of cyclin-dependent kinases (CDKs) were in fact quite potent on GSK-3 [24, 25]. Among these is a family of bis-indoles known as indirubins, initially identified as CDK inhibitors [26, 27]. Indirubins derive

from the spontaneous, nonenzymatic dimerization of isatin and indoxyl, two colorless precursors found either free or conjugated to carbohydrates, which are found in over 200 species of indigo-producing plants [28, 29]. Although they constitute minor side products, indirubins contribute by their red color to the unique blue-purplish color of natural indigo that distinguishes it from synthetic indigo. Indirubins, along with indigo, are also produced by various bacterial strains (reviewed in [30, 31]) and by a number of gastropod mollusks [32]. Moreover, they can be found in urine from diseased and healthy patients ([33] and references therein). Indirubin constitutes the main active ingredient of a traditional Chinese medicinal recipe, Danggui Longhui Wan, used to treat various diseases including chronic myelocytic leukemia [34, 35]. Indirubin and indigo have been recently discovered as potent ligands of the aryl hydrocarbon receptor (AhR), also known as the "dioxin receptor" [33] (M.K. et al., submitted).

Gastropods of the *Muricidae* and *Thaididae* families have been used in various parts of the world as the source of a vivid purplish-red dye known as "Tyrian purple" or "royal blue" around the Mediterranean sea [32]. The highly prized, beautiful Tyrian purple, obtained at great expense essentially from the two species *Murex brandaris* and *Hexaplex trunculus*, was the object of an important trade in Crete (5th century BC), Phoenicia, Greece, and later in Rome. The color was considered a privilege of the emperors Nero and Caligula. In Britain and Ireland, the dog whelk (*Nucella lapillus*) was also used for many years as a source of purple dye. Other dye-producing mollusks include *Purpura pansa* (Mexico, Pacific Ocean), *Purpura patula* (Mexico, Atlantic Ocean), and *Rapana venosa* (Japan). The hypobranchial gland of these gastropods contains colorless precursors, indoxyl-sulfate, its mercaptan derivative, and their bromo derivatives, which release various indoxyls upon maceration (in fact hydrolysis by purpurase). When exposed to light and oxygen, these indols dimerize in a mixture of indigo and indirubin, mainly 6,6′-dibromoindigo. Paul Friedlander was the first to determine the composition of the dye from *Murex brandaris*, in 1909, from 1.4 g of dye isolated from 12,000 mollusks [36]. The famous "Tekhelet" described in the Bible was also identified as a mixture of indigoids specifically obtained from *Hexaplex trunculus* [32, 37].

In an effort to identify new kinase inhibitors with increased potency and selectivity, we investigated the natural indirubins produced by the Mediterranean mollusk *Hexaplex trunculus*. Beside the dominant bromoindigos, we identified various bromo-substituted indirubins, and one of them, 6-bromoindirubin, which was isolated for the first time as a natural product, turned out to be a potent GSK-3 inhibitor. Its synthetic derivative, 6-bromoindirubin-3′-oxime (**BIO**), and related analogs constitute unique cell-permeable and selective inhibitors of GSK-3. We here provide the first cocrystal structures of GSK-3 and CDK5 with an inhibitor.

Results

Purification, Identification, and Kinase Inhibitory Properties of Shellfish Indirubins

Sixty kilograms of *Hexaplex trunculus* were collected, and the animals were extracted from the shells and exposed to sunlight to generate the expected Tyrian purple dye (Figure 1). The mollusks were then frozen and lyophilized prior to extraction by dichloromethane. Organic phase soluble indigoids were resolved by silica gel chromatography. Indigo derivatives were discarded, and indirubins (0.000025%) were further separated by MPLC and identified by 1D and 2D NMR and mass spectrometry as indirubin (**1**), 6′-bromoindirubin (**2**), 6-bromoindirubin (**3**), and 6,6′-dibromoindirubin (**4**) (Figure 1). 6-bromoindirubin (**3**) has never been isolated from any *Muricidae* or *Thaididae* gastropod or from any other natural source [32]. Each of these compounds was synthesized, along with its corresponding 3′-oxime derivative (**5–8**), as this modification enhances solubility, kinase inhibition, and cell permeability [24, 26]. 1-methyl derivatives (**9–11**) were also synthesized, as they were expected, from previous CDK2/indirubin cocrystal structures [26, 27], to provide kinase inactive control compounds. Finally, 3′-oxime in compound (**7**) was also replaced by 3′-methoxime (**12**) or 3′-acetoxime (**13**). We next evaluated the effects of these compounds on purified GSK-3α/β, CDK1/cyclin B, and CDK5/p25 (Table 1A). As expected, indirubin (**1**) was active on GSK-3α/β and on CDKs (10-fold less). Although a 6′-bromo substitution (**2**) led to reduced kinase inhibition, the 6-bromo substitution (**3**) greatly enhanced the selectivity for GSK-3 over CDKs. Addition of a 3′-oxime substitution (**5–8**) led to an overall increase in kinase inhibitory effects and increased solubility, although the selectivity for GSK-3 was slightly reduced. The 6-bromoindirubins substituted on 3′ by methoxime (**12**) or acetoxime (**13**) were also quite potent and GSK-3 selective (but less soluble, which precluded their use in cells). As expected, methylation on position N1 inactivated the indirubins (**9–11**) as kinase inhibitors.

6-Bromoindirubins Are Selective Inhibitors of GSK-3

We next tested **BIO** (**7**) and methoxime and acetoxime (**12, 13**) on a series of 20 purified protein kinases assayed in the presence of 15 μM ATP. The results of these assays confirm the strong selectivity of 6-bromo-substituted indirubins for GSK-3α/β (Table 1B). An acetoxime or methoxime substitution on position N3′ further contributes to the GSK-3 selectivity. As an alternative approach to evaluate the selectivity of **BIO**, we immobilized indirubin-3′-oxime on Affigel beads through a polyethylene linker attached at the 3′ position (Figures 2A and 2B). A porcine brain extract was then run on these beads in the absence or presence of free **BIO**, and the bound proteins were resolved by SDS-PAGE followed by silver staining and anti-GSK-3 Western blotting (Figures 2C and 2D). Although a large number of proteins were found to bind to indirubin beads, the presence of free **BIO** did not lead to major changes in the overall pattern of indirubin binding proteins. However, it completely prevented the binding of GSK-3α/β.

Cocrystal Structure of BIO with GSK-3β

We next attempted to soak **BIO** into a GSK-3β crystal, the structure of which had recently been described [38, 39]. A cocrystal structure was obtained with 2.8 Å resolution (Figure 3). The overall structure of GSK-3β/

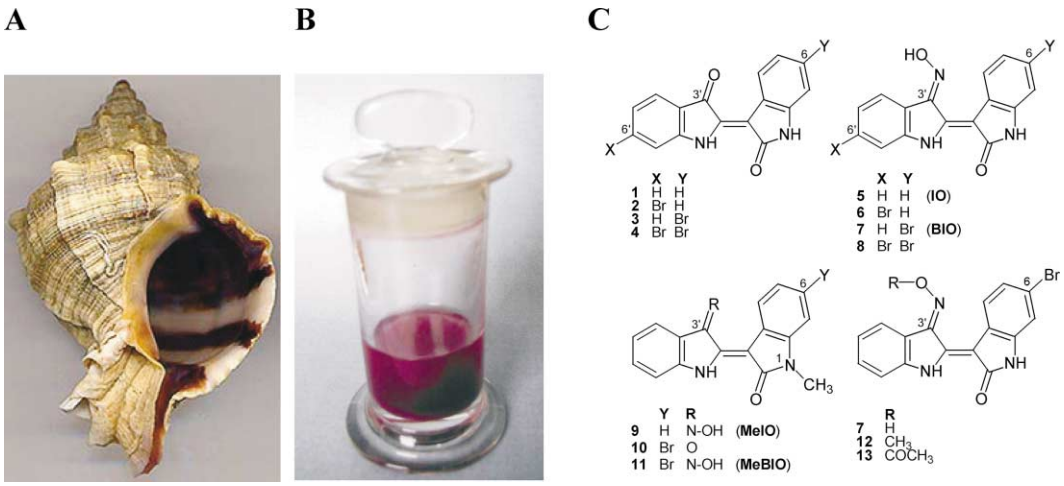

Figure 1. Tyrian Purple Constituents and Chemically Synthesized Indirubin Analogs

Hexaplex trunculus (A) was extracted for Tyrian purple (B), various brominated indirubins (**1–4**) (C), and indigos. Oxime derivatives (**5–8**) and N1-methylated analogs (**9–11**) of these indirubins were synthesized, as well as the methoxime and acetoxime of 6-bromoindirubin (**12, 13**). 6-bromoindirubin-3′-oxime (**BIO**) (**7**) and its control analog 1-methyl-6-bromoindirubin-3′-oxime (**MeBIO**) (**11**) were used in the biological models.

BIO is basically identical to the GSK-3β structure. The small N-terminal lobe of GSK-3β consists predominantly of β sheets, while the C-terminal lobe is predominantly α-helical (Figure 3A). **BIO** is located in the ATP binding pocket (Figure 3B). **BIO** binds in a planar conformation into a narrow hydrophobic pocket whose faces are defined by Ile62, Val70, Ala83, Leu132, and Tyr134 on one side and Thr138, Arg141, Leu188, and Cys199 on the other. As observed with CDK5-bound indirubin (see below), all direct hydrogen bonding interactions between **BIO** and the protein are made to the peptide backbone only and do not involve protein side chains. The cyclic nitrogen of the pyrole ring donates a hydrogen bond to the peptide carbonyl oxygen of Val135, while the cyclic nitrogen of the lactam ring donates a hydrogen bond to the carbonyl oxygen of Asp133, and the lactam carbonyl oxygen accepts a hydrogen bond from the backbone amide of Val135. As with CDK5, the bond to the backbone amide is quite short at around 2.4 Å. The preference of **BIO** for binding to GSK-3β as compared to CDKs can be explained by the presence of Leu132 in GSK-3β, which is in van der Waals contact with the bromine at one end of the pocket. In CDK2 and CDK5, the equivalent residue is a phenylalanine whose greater bulk would significantly hinder the binding of a bromine substituent at this position.

Cocrystal Structure of IO with CDK5/p25

As a complement to the CDK2/ indirubin cocrystal structures [26, 27] and for comparison, indirubin-3′-oxime (**IO**) (**5**) was cocrystallized with CDK5/p25, another major brain protein kinase involved, along with GSK-3, in the abnormal phosphorylation of tau in Alzheimer's disease. The overall structure of the CDK5/p25-**IO** complex is basically identical to the CDK5/p25 structure [40] (Figure 4A). The small N-terminal lobe of CDK5 consists predominantly of β sheets, while the C-terminal lobe is predominantly α-helical (Figure 4A). There are no significant differences in the reciprocal orientation of these lobes between the inhibitor-bound and the native complex. An "omit" map shows clear electron density for all inhibitor atoms (Figure 4B). **IO** binds in the ATP binding pocket of CDK5. The double-ring system of **IO** is inserted in a hydrophobic pocket formed by CDK5 residues Ile10, Val18, Ala31, Val64, Phe80, Leu133, and the alkyl portion of Asn144, and several van der Waals contacts are observed. In addition, three hydrogen bonds are formed with the backbone of CDK5. The N1′ cyclic nitrogen donates a hydrogen bond to the carbonyl oxygen of $Cys83^{CDK5}$, the carbonyl oxygen of the lactamic ring binds the backbone amide of $Cys83^{CDK5}$, and the N1 lactam amide nitrogen donates a hydrogen bond to the peptide oxygen of $Glu81^{CDK5}$ (Figure 4C). We next compared the CDK5 region involved in **IO** binding with the equivalent CDK2 region of the CDK2/cyclinA/indirubin-5-sulphonate (**I5S**) structure [27]. As shown in Figure 4D, the aromatic ring systems of both compounds occupy the same position in the two structures. This position provides optimal shape complementarity with the ATP binding cleft while allowing the formation of three hydrogen bonds with the backbone of residues 81 and 83. However, while the oxime group of **IO** makes no direct interactions with CDK5, the sulphonate group of **I5S** forms a salt bridge with $Lys33^{CDK2}$ and a hydrogen bond with the backbone nitrogen of $Asp145^{CDK2}$. These additional interactions may explain the higher affinity of **I5S** for both CDK5/p35 and CDK2/cyclinA (with IC_{50} values of 0.06 μM and 0.03 μM, respectively) relative to **IO** (0.10 μM and 0.44 μM, respectively) [26]. The nearly identical orientation of these inhibitors indicates that the effect of substitutions at the C3′ and C5 positions may be additive, suggesting a strategy for further improvement of these inhibitors.

6-Bromoindirubins Behave as GSK-3 Inhibitors in Cells

To test whether **BIO** behaved as a GSK-3 modulator in a cellular context, we measured its effects on the

Table 1. Selectivity of Tyrian Purple-Derived Indirubins

A. Effect of Indirubins on CDK1/Cyclin B, CDK5/p25, and GSK-3 Kinase Activities[a]

No.	Compound	GSK-3 α/β	CDK1/Cyclin B	CDK5/p25
1	indirubin	1.00	10.00	10.00
2	6′-bromoindirubin	22.00	>100.00	>100.00
3	6-bromoindirubin	0.045	90.00	53.00
4	6,6′-dibromoindirubin	4.50	100.00	>100.00
5	indirubin-3′-oxime (**IO**)	0.022	0.18	0.10
6	6′-bromoindirubin-3′-oxime	0.34	3.00	1.20
7	6-bromoindirubin-3′-oxime (**BIO**)	0.005	0.32	0.083
8	6,6′-dibromoindirubin-3′-oxime	0.12	17.00	1.30
9	1-methyl-indirubin-3′-oxime (**MeIO**)	>100.00	73.00	>100.00
10	1-methyl-6-bromoindirubin	>100.00	80.00	>100.00
11	1-methyl-6-bromoindirubin-3′-oxime (**MeBIO**)	44.00	55.00	>100.00
12	6-bromoindirubin-3′-methoxime	0.03	3.40	2.20
13	6-bromoindirubin-3′-acetoxime	0.01	63.00	2.40

B. Selectivity of 6-Bromoindirubins[b]

Protein Kinases	**5 (IO)**[c]	**7 (BIO)**	**12**	**13**
GSK-3α/β	0.022	0.005	0.030	0.010
CDK1/cyclin B	0.18	0.32	3.40	63
CDK2/cyclin A	0.44	0.30	15	4.3
CDK4/cyclin D1	3.33	10	>10	>10
CDK5/p35	0.10	0.08	2.20	2.4
erk1	>100	>10	>10	>10
erk2	>100	>10	>10	>10
MAPKK	>100	10	>10	>10
protein kinase C α	27	12	>10	>10
protein kinase C β1	4	>10	>10	>10
protein kinase C β2	20	>10	>10	>10
protein kinase C γ	8.40	>10	>10	>10
protein kinase C δ	>100	>10	>10	>10
protein kinase C ε	20	>10	>10	>10
protein kinase C η	52	>10	>10	>10
protein kinase C ζ	>100	>10	>10	>10
cAMP-dependent PK	6.3	>10	>10	>10
cGMP-dependent PK	9	>10	>10	>10
casein kinase 2	12	>10	9	>10
insulin receptor Tyr kinase	11	>10	>10	>10

[a] A series of indirubin analogs were tested at various concentrations in three kinase assays, as described in Experimental Procedures. IC_{50} values were calculated from the dose-response curves and are reported in μM.
[b] Kinases were assayed in the presence of various concentrations of each compound. IC_{50} values, determined from the dose-response curves, are expressed in μM.
[c] Data from [26].

phosphorylation of specific GSK-3 substrates. First, we made use of the monoclonal ABC antibody, a dephospho-specific antibody that crossreacts with β-catenin when it is not phosphorylated by GSK-3 (on either Ser37 or Thr41) [41]. This antibody thus provides a convenient positive signal on Western blots when GSK-3 is inhibited. We also made use of a general anti-β-catenin antibody, as inhibition of β-catenin phosphorylation leads to its stabilization [42]. COS-1 cells were exposed for 24 hr to various indirubins or to LiCl, and their levels of unphosphorylated β-catenin, total β-catenin, and total GSK-3 were examined by Western blotting (Figure 5A). **BIO** and LiCl treatment, but neither the kinase-inactive **MeBIO** nor **IO**, led to a major increase of the unphosphorylated β-catenin level. This was also accompanied by a modest increase in total β-catenin level, as expected from the dephosphorylation-dependent increased half-life of β-catenin. **BIO** thus acted as a true GSK-3 inhibitor in this cell line. The apparent lack of effect of **IO** in this cell line may be due to its reduced specificity compared to **BIO**, and therefore to its binding to alternative targets.

Indirubins have recently been described to interact with AhR [33]. To rule out the possibility that **BIO**-induced β-catenin dephosphorylation/stabilization was due to an indirect, AhR-dependent effect, we made use of cell lines deficient either in AhR or ARNT (a cotranscriptional factor of AhR) [43]. **BIO** triggered a robust β-catenin stabilization in both cell lines (Figure 5B). Furthermore, although **MeBIO** is a potent AhR agonist (M.K. et al., submitted), **MeBIO** is inactive on GSK-3β (Table 1A) and on cellular β-catenin phosphorylation/stabilization (Figure 5). Altogether, these data demonstrate that **BIO** acts by a direct effect on GSK-3 rather than through an indirect, AhR-dependent pathway.

GSK-3α and GSK-3β activity are enhanced by the phosphorylation of a specific tyrosine residue (Tyr276 and Tyr216, respectively) [44, 45]. The tyrosine kinase responsible for this phosphorylation in mammals is yet unknown, but there is some evidence that it indirectly

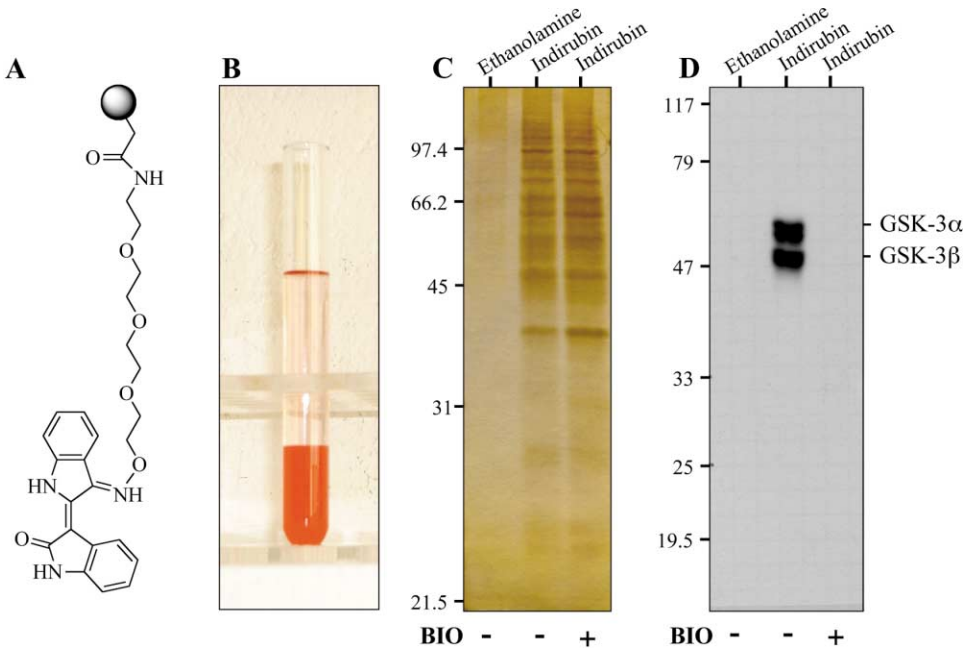

Figure 2. BIO Is a Selective GSK-3 Inhibitor In Vitro

Indirubin was immobilized on Affigel through a linker (A). Indirubin beads (B) and control ethanolamine beads were exposed to a porcine brain lysate in the presence (+) or absence (−) of 20 μM **BIO**. Following stringent washing, the bound proteins were analyzed by SDS-PAGE followed by silver staining (C) or Western blotting with anti-GSK-3 antibody (D).

depends on GSK-3 activity [11, 46]. We therefore investigated the effect of indirubins on this key tyrosine phosphorylation. SH-SY5Y cells were exposed to **IO**, **MeIO**, **BIO**, and **MeBIO** for 12 hr, and the phosphorylation of Tyr276 (GSK-3α) and Tyr216 (GSK-3β) was estimated by Western blotting with phospho-specific antibodies. As little as 1 μM **IO** and **BIO** dramatically reduced the level of tyrosine phosphorylation of both GSK-3 isoforms (Figure 5C). This was accompanied, as expected, by an increased level in total GSK-3β, total β-catenin, and dephospho-β-catenin. None of these changes were observed with **MeIO** and **MeBIO**.

6-Bromoindirubins Behave as GSK-3 Inhibitors In Vivo

We then investigated the in vivo effect of **BIO** in a well-known developmental system. GSK-3 is a component of the Wnt signal transduction pathway, where its phosphorylation of β-catenin inhibits signaling in the absence of Wnt ligand (Figure 6A) [42]. In *Xenopus laevis* embryos, maternal Wnt activity is necessary for dorsal axis formation, while inhibition of zygotic Wnt activity is required for head formation [47]. We compared the phenotypes of embryos treated with **BIO** or LiCl (Figures 6B–6G). When applied during early cleavage stage, LiCl leads to a hyper dorso-anteriorization at the expense of trunk and tail (anteriorized phenotype, Figure 6D). **BIO** phenocopies the LiCl effect in a dose-dependent manner (Figures 6E and 6F), while **MeBIO** remains without effect (Figure 6C). The Wnt pathway can ectopically induce dorsal genes, like the direct Wnt target *siamois* [48], and the Spemann organizer marker and *siamois* target *chordin* [49]. RT-PCR analysis of animal cap explants treated with LiCl (Figure 6H, lane 3) or **BIO** (lane 4) shows induction of both genes. This effect was resistant to injection of RNA encoding the Wnt inhibitor *axin* (Figure 6H, lanes 9 and 10), which requires GSK-3 for its activity, but not to a dominant-negative Tcf molecule (DN Xtcf-3) [50] (lanes 6 and 7) which blocks the pathway downstream of GSK-3 (Figure 6A). Another outcome of ectopic Wnt pathway activation in *Xenopus* is the indirect induction of neural tissue in animal cap explants [51]. We compared such explants from embryos treated with LiCl (Figure 6I, lanes 4 and 5), **BIO** (lanes 6 and 7), or injected with RNA for the neuralizing factor *noggin* (lane 3) by RT-PCR for various neural and anterior markers. **BIO** had the strongest effect on anterior markers like the neural gene *otx2* and the cement gland marker *xag1* even at the lowest concentration tested (5 μM). We conclude that **BIO** is an effective and specific inhibitor of GSK-3 activity in vivo, with higher specific activity than LiCl.

Discussion

Indirubins have been known for over a century as a contaminant of the plant-derived indigo dye. They can be obtained from plants, mollusks, bacteria, and mammalian urine. A few years ago, we discovered their potent action as protein kinase inhibitors, first on CDKs [26] and later on GSK-3 (24). In this article, we report that a minor modification (substitution on position 6) leads to enhanced selectivity for GSK-3 over CDKs. Compared to the nonsubstituted indirubins [26, 52], the bromine substitution appears to impart increased global selectivity as seen from the lack of effects of 6-bromo-

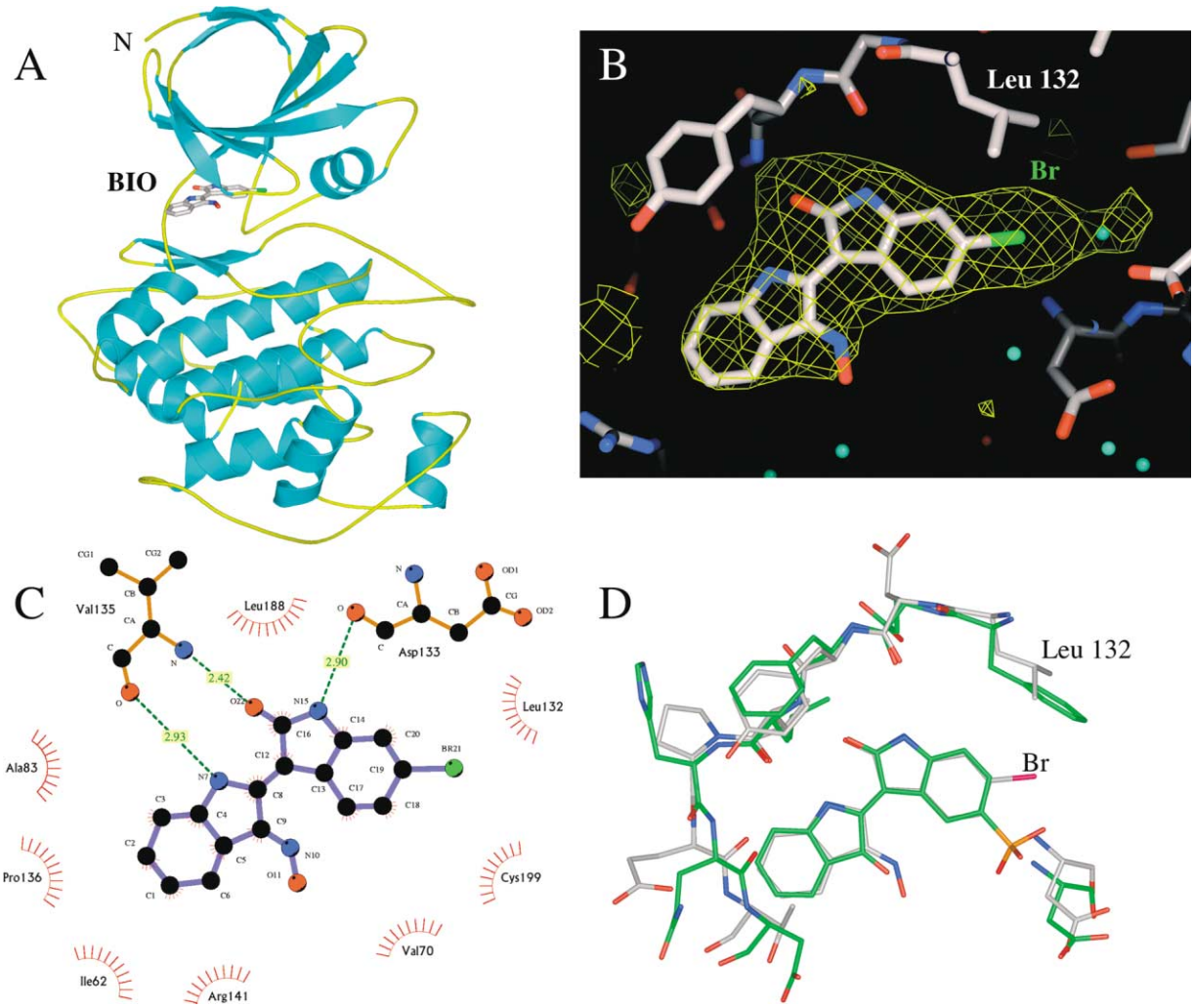

Figure 3. Structure of GSK-3β-BIO Cocrystal

(A) Ribbon diagram showing the overall fold of the GSK-3β-**BIO** complex. The **BIO** molecule is shown as a stick model with carbon atoms colored light gray, oxygen atoms red, nitrogen atoms blue, and bromine in green. The position of the N terminus is indicated.

(B) A $2F_o$-F_c omit density map of the **BIO** contoured at 2σ.

(C) LIGPLOT [65] interaction diagram for **BIO**. Hydrogen bonds are shown as dotted lines. Van der Waals contacts are shown as "hairy" semicircles.

(D) Superposition of CDK2/cyclinA-**I5S** with GSK-3β-**BIO**. The CDK complex is in green, and the GSK-3 complex is in gray. (A), (B), and (D) were created with PyMol [66].

substituted indirubins on a large panel of kinases (Table 1B) and from the affinity chromatography experiment (Figure 2). The reasons behind this unexpected specificity for GSK-3 became clear when the GSK-3β/**BIO** and CDK5/**IO** or CDK2/**IO** cocrystal structures were examined. Briefly, the bromine of **BIO** establishes a van der Waals contact with the Leu132 residue of GSK-3. The corresponding amino acid in CDK2 and CDK5 is a phenylalanine, i.e., a bulkier residue, which would prohibit the binding of the bromine. In addition, the position 5 of indirubin could probably accommodate another small substitution compatible with binding to GSK-3 but not to CDKs. A more extensive discussion of the structure/activity relationship of indirubins will be presented elsewhere (P.M. et al., unpublished data). We feel that further exploration of the 5 and 6 positions in indirubins is likely to give access to further potent and selective inhibitors of GSK-3. It should also provide the opportunity to improve the solubility of these hydrophobic compounds and to improve their pharmacokinetic properties. As many ATP-competitive kinase inhibitors bind by hydrophobic interactions within the ATP binding pocket of their kinase targets [53], they are bound to be rather hydrophobic, poorly soluble compounds, and this profile needs to be improved for clinical applications.

Interestingly, indirubins were found to inhibit the phosphorylation of Tyr276/Tyr216 (GSK-3α/GSK-3β) (Figure 5C), further contributing to the inactivation of GSK-3 activity. It is unlikely that GSK-3, a Ser/Thr kinase, phosphorylates itself on this Tyr residue. Furthermore, a kinase-inactive GSK-3β mutant was phosphorylated on Tyr216 following apoptotic stimuli [11]. It is possible that

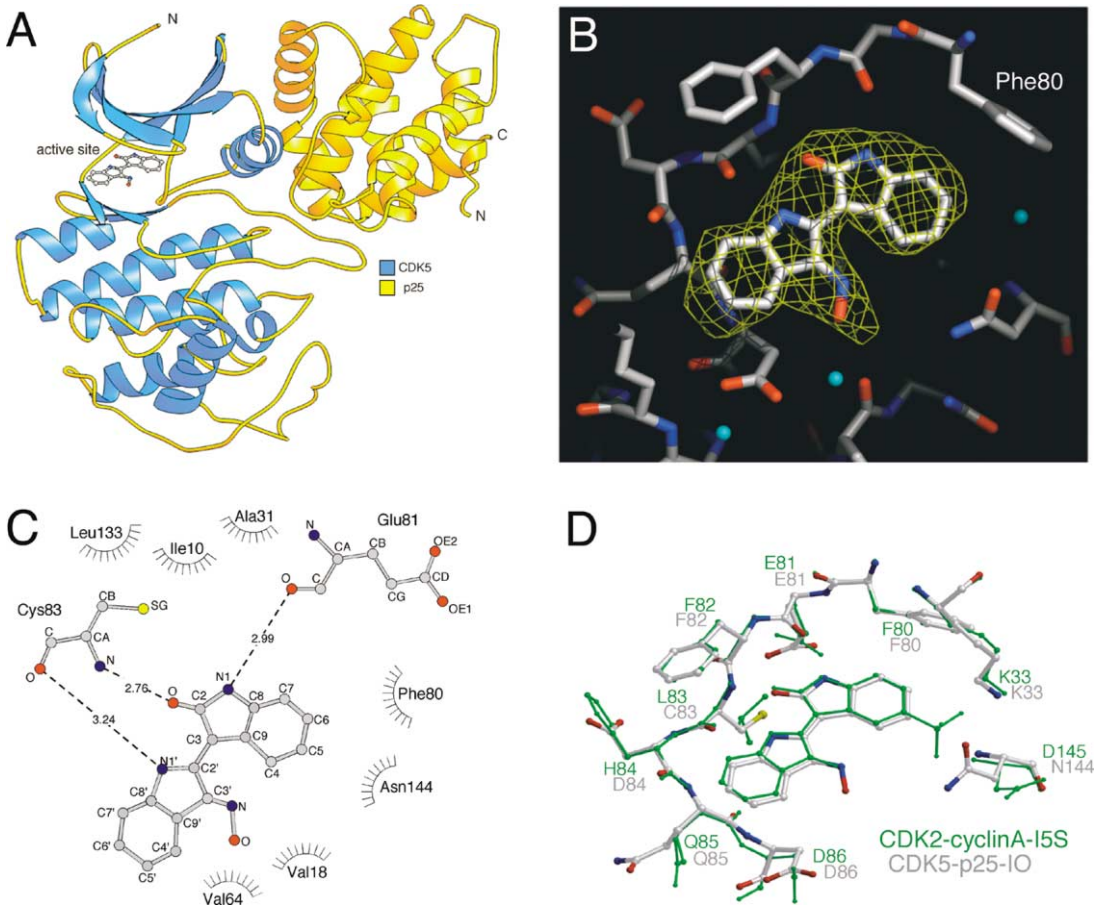

Figure 4. Structure of CDK5/p25-IO Cocrystal

(A) Ribbon diagram showing the overall fold of the CDK5/p25-**IO** complex. The **IO** molecule is shown in a ball-and-stick representation with carbon atoms colored light gray, oxygen atoms red, and nitrogen atoms blue. The position of the N and C termini are indicated. The figure was created with the program RIBBONS [67].

(B) A $2F_o$-F_c omit electron density map for **IO** contoured at one time the root mean square deviation (1 σ) of the map.

(C) Schematic diagram of the interaction of **IO** with CDK5/p25. Hydrogen bonds are shown as dotted lines. Van der Waals contacts are shown as "hairy" semicircles. The diagram was created with the program LIGPLOT [65].

(D) Superposition of CDK5/p25-**IO** and CDK2/cyclinA-**I5S** obtained considering the kinase residues adjacent to the inhibitors. **IO** is colored as in (A), while atoms in CDK2/cyclinA-**I5S** are colored green.

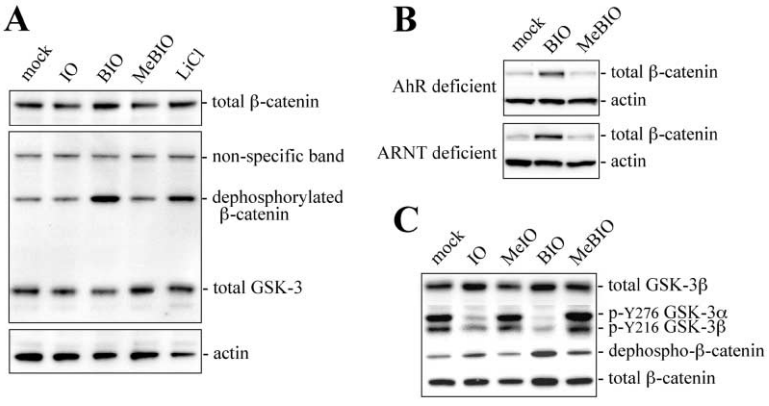

Figure 5. BIO Is a Selective GSK-3 Inhibitor in Cell Cultures

(A) **BIO** inhibits the phosphorylation of β-catenin on GSK-3-specific sites. Cos-1 cells were untreated (mock) or exposed to 5 μM **IO**, **BIO**, **MeBIO**, or 20 mM LiCl for 24 hr. Proteins were then separated by SDS-PAGE followed by Western blotting with antibodies directed (top to bottom) against β-catenin, dephospho-β-catenin, GSK-3, and actin (loading control). A nonspecific band detected with the dephospho-β-catenin was used as an additional loading control.

(B) Independence from AhR. Cell lines deficient either for AhR or ARNT were exposed to 10 μM **BIO** and 50 μM **MeBIO** for 24 hr. Western blots were then made with antibodies directed against β-catenin and actin (loading control).

(C) Indirubins inhibit the tyrosine phosphorylation of GSK-3. SH-SY5Y cells were untreated (mock) or exposed to 1 μM **IO**, **MeIO**, **BIO**, and **MeBIO** for 12 hr. Proteins were then separated by SDS-PAGE followed by Western blotting with antibodies directed (top to bottom) against total GSK-3β, phospho Tyr276 (GSK-3α)/Tyr216 (GSK-3β), dephospho-β-catenin, and total β-catenin.

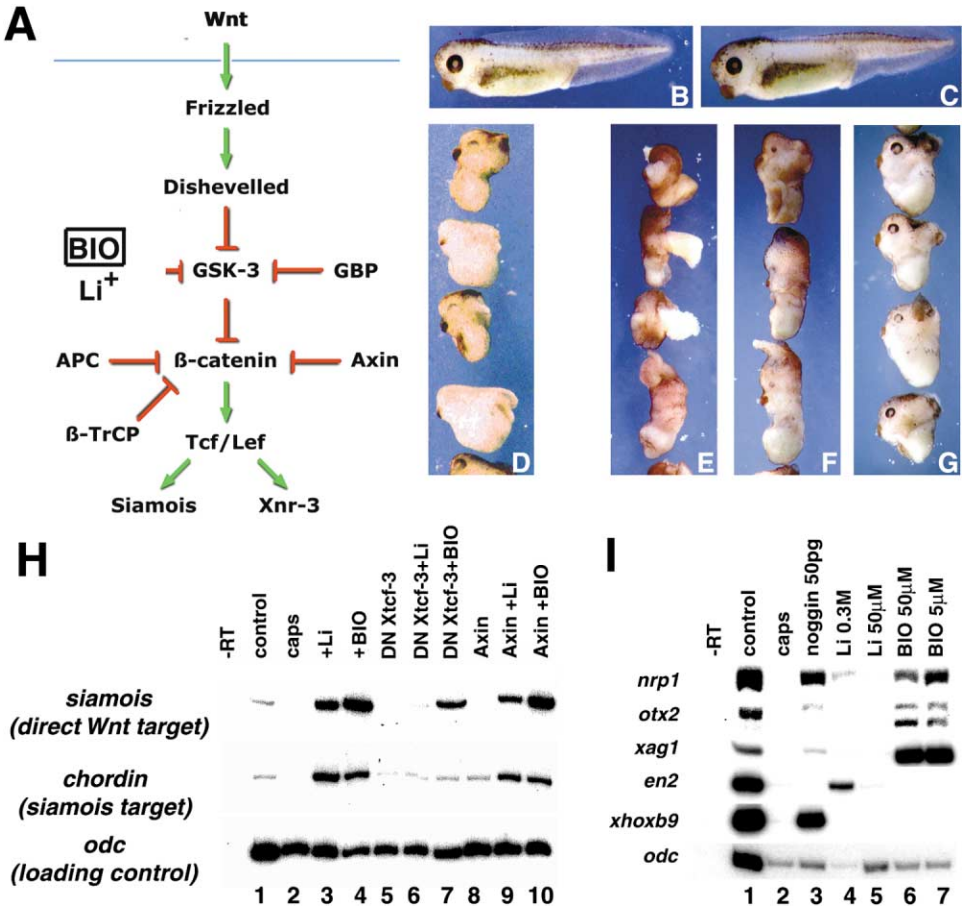

Figure 6. BIO Activates the Maternal Wnt Signaling Pathway in *Xenopus laevis* Embryos

(A) Diagram of the Wnt pathway in *Xenopus*. The site of action and mechanism for Wnt pathway activation are indicated. Green arrows indicate positive effects, and red capped lines indicate negative ones.

(B) Untreated embryo, tadpole stage.

(C–G) Activation of the maternal Wnt pathway. Embryos were treated with the specified reagents before stage 8, and were allowed to develop to tadpole stage. (C), embryos treated with 50 μM of the inactive **MeBIO** are unchanged; (D) embryos treated with 0.3 M LiCl are anteriorized. (E)–(G) demonstrate the dose-dependent effect of **BIO**. The intensity of the anteriorized phenotype increases with **BIO** concentration (50 μM, 15 μM, and 5 μM, respectively).

(H) **BIO** activates ectopically the dorsal genes *siamois* and *chordin*, and epistasis analysis of their induction is consistent with in vivo inhibition of GSK-3. RT-PCR of animal cap explants for the direct Wnt target gene *siamois* and the *siamois* target *chordin* with *odc* as loading control. Li^+ (0.3 M) and **BIO** (50 μM) induce both *siamois* and *chordin* (lanes 3 and 4), which are absent in explants from untreated embryos (lane 2). The GSK-3-independent inhibitor of the Wnt pathway DN-Xtcf-3 completely blocks the effect of Li^+ (lane 6) and partially blocks the effect of **BIO** (lane 7). The GSK-3-dependent inhibitor axin fails to block either Li^+ (lane 9, compare to lane 3) or **BIO** (lane 10, compare to lane 4).

(I) **BIO** is a potent anterior and neural tissue inducer in animal cap explants. RT-PCR of animal cap explants for general neural (*nrp1*), anterior neural (*otx2*), anterior tissue (cement gland marker *xag1*), midbrain (*en2*), and posterior neural (*xhoxb9*) markers. Lane 1 is a control embryo, stage 16. Cap explants from untreated embryos do not express anterior or neural markers (lane 2). Animal cap explants from embryos treated with **BIO** (lanes 6 and 7) express anterior neural markers more effectively than explants from embryos treated with LiCl (lanes 4 and 5) or injected with RNA for the neural inducer *noggin* (lane 3). *odc* is a loading control marker.

the presence of indirubin in the ATP binding pocket of GSK-3 prohibits access to the tyrosine kinase responsible for Tyr216/276 phosphorylation. This steric hindrance may thus lead to a secondary inhibitory effect on GSK-3. Another possibility is that the tyrosine kinase phosphorylating Tyr276/Tyr216 is downstream of GSK3α/GSK-3β in a feedback pathway, such that inhibition of GSK-3 by indirubins prevents the activation of the GSK-3 kinase that acts upon these tyrosine residues.

From the diverse available kinase/indirubin cocrystal structures, we were able to generate indirubins (such as **MeIO** and **MeBIO**) that are unable to inhibit the kinases, simply by introducing a methyl substitution on N1. These compounds could be useful as controls but also as molecular sinks to neutralize nonkinase, indirubin binding proteins such as AhR. Unfortunately, the 1-methylated indirubins are rather active AhR agonists, and this should be taken into account. So far, we have been unable to generate indirubin analogs that are active on the kinases but totally inactive on AhR (M.K. et al., submitted).

There is a strong need for pharmacological inhibitors to probe the multiple functions of GSK-3 in cell physiology. Only a limited number of such inhibitors are avail-

able (reviewed in [21, 54, 55]), and their selectivity is usually uncharacterized. **BIO**, **MeBIO**, and related indirubins thus provide potent, micromolar pharmacological tools, as well as relevant inactive controls, to investigate the cellular functions of GSK-3. However, in addition to these indirubins the parallel use of other reported, structurally unrelated, GSK-3 inhibitors would help to probe the involvement of GSK-3 in cellular processes. In this context, the combined use of kenpaullone [54] and lithium has been recently recommended [52].

Pharmacological inhibitors of GSK-3 are being developed as potential drugs against diabetes, neurodegenerative diseases, cancer, inflammation, and infectious diseases. We are currently interested in the implication of GSK-3 in neurodegenerative disorders, which are associated with neuronal cell death, such as Alzheimer's disease (see Introduction; reviewed in [56]). Indeed, the two main diagnostic features of Alzheimer's disease, β-amyloid toxicity/agregation and tau hyperphosphorylation/aggregation, are both directly linked to GSK-3 (reviewed in [4, 56, 57]). β-amyloid aggregates induce the activation of GSK-3 and apoptotic cell death, and this is prevented by lithium ([58–60] and references therein). Very recently, a role for GSK-3α in the production of β-amyloid peptides was demonstrated [61]. Inhibition of GSK-3 by lithium, kenpaullone, or RNAi resulted in a dramatic decrease in β-amyloid production [61]. Aggregation of the microtubule binding protein tau is directly linked to hyperphosphorylation by two main enzymes, CDK5/p25 and GSK-3. GSK-3 is one of the enzymes responsible for the appearance of Alzheimer's disease-specific epitopes in tau [4, 62, 63]. Altogether, these data support the validity of evaluating pharmacological inhibitors of GSK-3 for the treatment of Alzheimer's disease. The cocrystal structure of GSK-3β and an inhibitor presented here provides tools for molecular modeling of new inhibitors.

Significance

The bis-indole indirubin has been known for over a century as a contaminant of the plant-derived indigo dye. It also constitutes the active ingredient of a traditional Chinese medicinal recipe used to treat chronic myelocytic leukemia. We here show that 6-brominated indirubins extracted from another natural source, the Mollusk *Hexaplex trunculus*, provide an unexpected scaffold to generate potent kinase inhibitors selective for GSK-3 as compared to CDKs. We also provide cocrystal structures of indirubins in complex with GSK-3 and CDK5. These 6-brominated indirubins may be useful as pharmacological tools in cell biology. Furthermore, they could be used to investigate the effects of GSK-3 modulation on the long-term outcome of neurodegenerative diseases such as Alzheimer's disease and other diseases such as diabetes.

Experimental Procedures

Natural Products Extraction and Chemistry

General Chemistry Experimental Procedures

NMR spectra were recorded on Bruker DRX 400 and Bruker AC 200 spectrometers (^{1}H [400 and 200 MHz] and ^{13}C [50 MHz]); chemical shifts are expressed in ppm downfield from TMS. The ^{1}H-^{1}H and the ^{1}H-^{13}C NMR experiments were performed using standard Bruker microprograms. CI-MS spectra were determined on a Finnigan GCQ *Plus* ion-trap mass spectrometer using CH_4 as the CI ionization reagent. Medium pressure liquid chromatography (MPLC) was performed with a Büchi model 688 apparatus on columns containing Si gel 60 Merck (20–40 μm). Thin layer chromatography (TLC) was performed on plates coated with Si gel 60 F_{254} Merck, 0.25 mm. All the compounds gave satisfactory combustion analyses (C, H, N, within ± 0.4% of calculated values).

Biological Material

The marine mollusk *Hexaplex trunculus* L. was collected in shallow waters in the Saronikos gulf near the island of Salamina (Greece). Voucher specimens are deposited in the collection of the Goulandris Natural History Museum.

Extraction and Isolation of Indirubins

The mollusks (60 kg), after removal of the shells, were exposed to sunlight for 6 hr, lyophilized, and extracted with CH_2Cl_2 (3 × 15 liter for 48 hr). The CH_2Cl_2 extract (162 g) was subjected to vacuum liquid chromatography on silica gel 60H with increasing polarity mixtures of cyclohexane/CH_2Cl_2 (from 100:0 to 0:100) to afford 45 fractions of 500 ml. Fractions 34–45 were rechromatographed with vacuum liquid chromatography on silica gel 60H with increasing polarity mixtures of cyclohexane/EtOAc (from 95:5 to 0:100) to afford 40 fractions of 300 ml. Fractions 36–39 were submitted to medium pressure liquid chromatography (MPLC) using a cyclohexane/EtOAc gradient (from 95:5 to 85:15) to give indirubin (**1**) (3.5 mg), 6′-bromoindirubin (**2**) (5.5 mg), 6-bromoindirubin (**3**) (2.8 mg), and 6,6′-dibromoindirubin (**4**) (3 mg).

General Synthetic Procedures

The synthesis of indirubin precursors and indirubins is described in detail elsewhere (P.M. et al., unpublished data). Indirubin (**1**) was prepared from isatin and 3-acetoxyindol. 6′-bromoindirubin (**2**) was prepared from isatin and 3-acetoxy-6-bromoindol. 6-bromoindirubin (**3**) was prepared from 6-bromoisatin and 3-acetoxyindol. 6,6′-Dibromoindirubin (**4**) was prepared from 6-bromoisatin and 3-acetoxy-6-bromoindol. 6-bromo-1-methylindirubin (**10**) was prepared from 6-bromo-1-methylisatin and 3-acetoxyindol. Indirubin-3′-oxime (**5**) (**IO**), 6′-bromoindirubin-3′-oxime (**6**), 6-bromoindirubin-3′-oxime (**7**) (**BIO**), 6,6′-dibromoindirubin-3′-oxime (**8**), 1-methylindirubin-3′-oxime (**9**) (**MeIO**),and 1-methyl-6-bromoindirubin-3′-oxime (**11**) (**MeBIO**) were prepared from the corresponding indirubins (**1**, **2**, **3**, **4**, 1-methylindirubin, **10**) and hydroxylamine hydrochloride.

Kinase Assays

The preparation and assay of protein kinases is described in the Supplemental Data (http://www.chembiol.com/cgi/content/full/10/12/1255/DC1).

Affinity Chromatography on Immobilized Indirubin

The immobilization of indirubin on a matrix is described in the Supplemental Data (see URL above).

Preparation of Extracts

Pork brains were obtained from a local slaughterhouse and directly homogenized and processed for affinity chromatography or stored at −80°C prior to use. Tissues were weighed, homogenized, and sonicated in homogenization buffer (2 ml per g of material). Homogenates were centrifuged for 10 min at 14,000 × g at 4°C. The supernatant was recovered, assayed for protein content (BIO-Rad assay), and immediately loaded batchwise on the affinity matrix.

Affinity Chromatography of Interacting Proteins

Just before use, 20 μl of packed indirubin beads were washed with 1 ml of bead buffer (50 mM Tris [pH 7.4], 5 mM NaF, 250 mM NaCl, 5 mM EDTA, 5 mM EGTA, 0.1% Nonidet P-40, 10 μg leupeptin/ml, 10 μg aprotinin/ml, 10 μg soybean trypsin inhibitor/ml, and 100 μM benzamidine) and resuspended in 600 μl of this buffer. The tissue extract supernatant (4 mg total protein) was then added in the presence or absence of 20 μM **BIO**; the tubes were rotated at 4°C for 30 min. After a brief spin at 10,000 × g and removal of the supernatant, the beads were washed four times with bead buffer before addition of 50 μl of 2× Laemmli sample buffer.

Electrophoresis and Western Blotting

Following heat denaturation for 3 min, the proteins bound to the indirubin matrix were separated by 10% SDS-PAGE (0.7 mm thick

gels) followed by immunoblotting analysis or silver staining. Silver staining was performed according to a "home recipe" (fixative: 250 μl 37% formaldehyde in 250 ml 50% methanol; rinsing with milliQ water containing 35 μM DTT, followed by 0.1% $AgNO_3$ in milliQ water (w/v); developer: 12 g Na_2CO_3 in 400 ml milliQ water containing 200 μl 37% formaldehyde). For immunoblotting, proteins were transferred to 0.1 μm nitrocellulose filters (Schleicher and Schuell). These were blocked with 5% lowfat milk in Tris-Buffered Saline-Tween-20 (TBST), incubated with anti-GSK-3α/β (mouse monoclonal anti-GSK-3α/β antibody [KAM-ST002C], from StressGen Biotechnologies Corp.; 1:1000; 1 hr), and analyzed by Enhanced Chemiluminescence (ECL, Amersham).

Effects of Indirubins on Level and Phosphorylation of β-Catenin and GSK-3 in Cell Lines

COS1, Hepa (wild-type, CEM/LM AhR deficient and ELB1 ARNT deficient), or SH-SY5Y cells were grown in 6 cm culture dishes in Dulbecco's Modified Medium (DMEM) containing 10% fetal bovine serum (Invitrogen). For treatment, **IO** (5 μM), **BIO** (5 or 10 μM), **MeBIO** (5 or 50 μM), LiCl (20 or 40 mM), or mock solution (DMSO, 0.5% final concentration) was added to medium when cell density reached ~70% confluence. After 12 (SH-SY5Y) or 24 hr, the cells, while still in plate, were lysed with lysis buffer (1% SDS, 1 mM sodium orthovanadate, 10 mM Tris [pH 7.4]). The lysate was passed several times through a 26G needle, centrifuged at 10,000 × g for 5 min, and adjusted to equal protein concentration. About 8 μg of each sample was loaded for immunoblotting. Enhanced chemiluminescence (PerkinElmer) was used for detection. The following primary antibodies were used: mouse anti-β-catenin CT (Upstate Biotechnolgies, Clone 7D8, recognizes total β-catenin), mouse anti-phospho-β-catenin (Upstate Biotechnologies, Clone 8E7, recognizes dephosphorylated β-catenin) [41], mouse anti-GSK-3 β (BD Transduction Laboratories, 610201), mouse anti-GSK-3 phosphoTyr216 (Transduction Laboratories), rabbit anti-AhR (Aryl hydrocarbon receptor) (BIOMOL Research Laboratories, SA-210), and rabbit anti-actin (Sigma, A5060).

Effects of Indirubins on *Xenopus* Embryos

Handling of Embryos

Xenopus laevis embryos obtained by in vitro fertilization were cultured in 0.1× MMR and staged [64]. For lithium treatment, embryos were placed in 0.3 M LiCl solution for 10 min at the 16-cell stage. For experiments with **BIO**, the reagent was added to the indicated final concentrations at the 4-cell stage and washed away at stage 8. Embryos were subsequently allowed to develop to tadpole stage. RNA injections were performed at 2- to 4-cell stage with the indicated amounts of in vitro transcribed RNA in a 10 nl volume. Animal caps were dissected at blastula (stage 9) and cultured to neurula (stage 18) for RT-PCR analysis.

In Vitro Transcription and RT-PCR

The sequences of oligonucleotides used for RT-PCR are provided in the Supplemental Data (available at *Chemistry & Biology*'s website).

Acknowledgments

We thank Dr. J. Wang for the CDK5 and p25 clones and Drs. Xu Wu and Dr. Nathanael Gray for the indirubin resin. The photograph of *H. trunculus* is courtesy of Hervé Bordas and Giorgio Griffon and that of Tyrian purple by Stéphane Bach. This research was supported by the "Association pour la Recherche sur le Cancer" (ARC 5343 & ARC5732) (L.M.) and the Ministère de la Recherche/INSERM/CNRS "Molécules et Cibles Thérapeutiques" Programme. L.M.'s sabbatical leave in Dr. P. Greengard's laboratory was supported by the Rockefeller University and the CNRS.

Received: August 6, 2003
Revised: October 3, 2003
Accepted: October 6, 2003
Published: December 19, 2003

References

1. Cohen, P., and Frame, S. (2001). The renaissance of GSK3. Nat. Rev. Mol. Cell Biol. *2*, 769–776.
2. Grimes, C.A., and Jope, R.S. (2001). The multifaceted roles of glycogen synthase kinase 3 in cellular signaling. Prog. Neurobiol. *65*, 391–426.
3. Eldar-Finkelman, H. (2002). Glycogen synthase kinase 3: an emerging therapeutic target. Trends Mol. Med. *8*, 126–132.
4. Kaytor, M.D., and Orr, H.T. (2002). The GSK3β signaling cascade and neurodegenerative disease. Curr. Opin. Neurobiol. *12*, 275–278.
5. Doble, B.W., and Woodgett, J.R. (2003). GSK-3: tricks of the trade for a multi-tasking kinase. J. Cell Sci. *116*, 1175–1186.
6. Ding, Y., and Dale, T. (2002). Wnt signal transduction: kinase cogs in a nano-machine. Trends Biochem. Sci. *27*, 327–329.
7. Li, X., Bijur, G.N., and Jope, R.S. (2002). Glycogen synthase kinase-3beta, mood stabilizers, and neuroprotection. Bipolar Disord. *4*, 137–144.
8. Bijur, G.N., and Jope, R.S. (2001). Proapoptotic stimuli induce nuclear accumulation of glycogen synthase kinase-3 beta. J. Biol. Chem. *276*, 37436–37442.
9. Crowder, R.J., and Freeman, R.S. (2000). Glycogen synthase kinase-3 beta activity is critical for neuronal death caused by inhibiting phosphatidylinositol 3-kinase or Akt but not for death caused by nerve growth factor withdrawal. J. Biol. Chem. *275*, 34266–34271.
10. Culbert, A.A., Brown, M.J., Frame, S., Hagen, T., Cross, D.A., Bax, B., and Reith, A.D. (2001). GSK-3 inhibition by adenoviral FRAT1 overexpression is neuroprotective and induces Tau dephosphorylation and beta-catenin stabilisation without elevation of glycogen synthase activity. FEBS Lett. *507*, 288–294.
11. Bhat, R.V., Shanley, J., Correll, M.P., Fieles, W.E., Keith, R.A., Scott, C.W., and Lee, C.M. (2000). Regulation and localization of tyrosine216 phosphorylation of glycogen synthase kinase-3beta in cellular and animal models of neuronal degeneration. Proc. Natl. Acad. Sci. USA *97*, 11074–11079.
12. Cross, D.A., Culbert, A.A., Chalmers, K.A., Facci, L., Skaper, S.D., and Reith, A.D. (2001). Selective small-molecule inhibitors of glycogen synthase kinase-3 activity protect primary neurones from death. J. Neurochem. *77*, 94–102.
13. Bijur, G.N., De Sarno, P., and Jope, R.S. (2000). Glycogen synthase kinase-3beta facilitates staurosporine- and heat shock-induced apoptosis. Protection by lithium. J. Biol. Chem. *275*, 7583–7590.
14. Song, L., De Sarno, P., and Jope, R.S. (2002). Central role of glycogen synthase kinase-3beta in endoplasmic reticulum stress-induced caspase-3 activation. J. Biol. Chem. *277*, 44701–44708.
15. Carmichael, J., Sugars, K.L., Bao, Y.P., and Rubinsztein, D.C. (2002). Glycogen synthase kinase-3beta inhibitors prevent cellular polyglutamine toxicity caused by the Huntington's disease mutation. J. Biol. Chem. *277*, 33791–33798.
16. You, Z., Saims, D., Chen, S., Zhang, Z., Guttridge, D.C., Guan, K.L., MacDougald, O.A., Brown, A.M., Evan, G., Kitajewski, J., et al. (2002). Wnt signaling promotes oncogenic transformation by inhibiting c-Myc-induced apoptosis. J. Cell Biol. *157*, 429–440.
17. Hashimoto, M., Sagara, Y., Langford, D., Everall, I.P., Mallory, M., Everson, A., Digicaylioglu, M., and Masliah, E. (2002). Fibroblast growth factor 1 regulates signaling via the glycogen synthase kinase-3beta pathway. Implications for neuroprotection. J. Biol. Chem. *277*, 32985–32991.
18. Li, M., Wang, X., Meintzer, M.K., Laessig, T., Birnbaum, M.J., and Heidenreich, K.A. (2000). Cyclic AMP promotes neuronal survival by phosphorylation of glycogen synthase kinase 3beta. Mol. Cell. Biol. *20*, 9356–9363.
19. Lucas, J.J., Hernandez, F., Gomez-Ramos, P., Moran, M.A., Hen, R., and Avila, J. (2001). Decreased nuclear beta-catenin, tau hyperphosphorylation and neurodegeneration in GSK-3beta conditional transgenic mice. EMBO J. *20*, 27–39.
20. Jackson, G.R., Wiedau-Pazos, M., Sang, T.-K., Wagle, N., Brown, C.A., Massachi, S., and Geschwind, D.H. (2002). Human wild-type tau interacts with wingless pathway components and produces neurofibrillary pathology in Drosophila. Neuron *34*, 509–519.
21. Martinez, A., Castro, A., Dorronsoro, I., and Alonso, M. (2002). Glycogen synthase kinase 3 (GSK-3) inhibitors as new promising

drugs for diabetes, neurodegeneration, cancer, and inflammation. Med. Res. Rev. *22*, 373–384.

22. Davies, S.P., Reddy, H., Caivano, M., and Cohen, P. (2000). Specificity and mechanism of action of some commonly used protein kinase inhibitors. Biochem. J. *351*, 95–105.
23. Patel, S., Yenush, L., Rodriguez, P.L., Serrano, R., and Blundell, T.L. (2002). Crystal structure of an enzyme displaying both inositol-polyphosphate-1-phosphatase and 3′-phosphoadenosine-5′-phosphate phosphatase activities: a novel target of lithium therapy. J. Mol. Biol. *315*, 677–685.
24. Leclerc, S., Garnier, M., Hoessel, R., Marko, D., Bibb, J.A., Snyder, G.L., Greengard, P., Biernat, J., Wu, Y.Z., Mandelkow, E.-M., et al. (2001). Indirubins inhibit glycogen synthase kinase-3β and CDK5/p25, two kinases involved in abnormal tau phosphorylation in Alzheimer's disease–A property common to most CDK inhibitors? J. Biol. Chem. *276*, 251–260.
25. Knockaert, M., Viking, K., Schmitt, S., Leost, M., Mottram, J., Kunick, C., and Meijer, L. (2002). Intracellular targets of paullones: identification by affinity chromatography using immobilized inhibitor. J. Biol. Chem. *277*, 25493–25501.
26. Hoessel, R., Leclerc, S., Endicott, J., Noble, M., Lawrie, A., Tunnah, P., Leost, M., Damiens, E., Marie, D., Marko, D., et al. (1999). Indirubin, the active constituent of a Chinese antileukaemia medicine, inhibits cyclin-dependent kinases. Nat. Cell Biol. *1*, 60–67.
27. Davies, T.G., Tunnah, P., Meijer, L., Marko, D., Eisenbrand, G., Endicott, J.A., and Noble, M.E.M. (2001). Inhibitor binding to active and inactive CDK2. The crystal structure of a CDK2-cyclin A/indirubin-5-sulphonate. Structure *9*, 389–397.
28. Balfour-Paul, J. (1998). Indigo. (London:British Museum Press).
29. Maugard, T., Enaud, E., Choisy, P., and Legoy, M.D. (2001). Identification of an indigo precursor from leaves of Isatis tinctoria (Woad). Phytochemistry *58*, 897–904.
30. MacNeil, I.A., Tiong, C.L., Minor, C., August, P.R., Grossman, T.H., Loiacono, K.A., Lynch, B.A., Phillips, T., Narula, S., Sundaramoorthi, R., et al. (2001). Expression and isolation of antimicrobial small molecules from soil DNA libraries. J. Mol. Microbiol. Biotechnol. *3*, 301–308.
31. Gillam, E.M.J., Notley, L.M., Cai, H., DeVoss, J.J., and Guengerich, F.P. (2000). Oxidation of indole by cytochrome P450 enzymes. Biochemistry *39*, 13817–13824.
32. Cooksey, C.J. (2001). Tyrian purple: 6,6'-dibromoindigo and related compounds. Mol. *6*, 736–769.
33. Adachi, J., Mori, Y., Matsui, S., Takigami, H., Fujino, J., Kitagawa, H., Miller, C.A., 3rd, Kato, T., Saeki, K., and Matsuda, T. (2001). Indirubin and indigo are potent aryl hydrocarbon receptor ligands present in human urine. J. Biol. Chem. *276*, 31475–31478.
34. Tang, W., and Eisenbrand, G. (1992). Chinese Drugs of Plant Origin: Chemistry, Pharmacology, and Use in Traditional and Modern Medicine (Heidelberg, Germany: Springer-Verlag).
35. Xiao, Z., Hao, Y., Liu, B., and Qian, L. (2002). Indirubin and meisoindigo in the treatment of chronic myelogenous leukemia in China. Leuk. Lymphoma *43*, 1763–1768.
36. Friedländer, P. (1909). Uber den Farbstoff des antiken Purpurs aus Murex brandaris. Angew. Chem. *22*, 2492–2494.
37. Fouquet, H., and Bielig, H.J. (1971). Biological precursors and genesis of tyrian-purple. Angew. Chem. Int. Ed. Engl. *10*, 816–817.
38. Dajani, R., Fraser, E., Roe, S.M., Young, N., Good, V., Dale, T.C., and Pearl, L.H. (2001). Crystal structure of glycogen synthase kinase 3β: structural basis for phosphate-primed substrate specificity and autoinhibition. Cell *105*, 721–732.
39. ter Haar, E., Coll, J.T., Austen, D.A., Hsiao, H.M., Swenson, L., and Jain, J. (2001). Structure of GSK3β reveals a primed phosphorylation mechanism. Nat. Struct. Biol. *8*, 593–596.
40. Tarricone, C., Dhavan, R., Peng, J., Areces, L.B., Tsai, L.H., and Musacchio, A. (2001). Structure and regulation of the CDK5-p25^{nck5a} complex. Mol. Cell *8*, 657–669.
41. van Noort, M., Meeldijk, J., van der Zee, R., Destree, O., and Clevers, H. (2002). Wnt signaling controls the phosphorylation status of beta-catenin. J. Biol. Chem. *277*, 17901–17905.
42. Huelsken, J., and Birchmeier, W. (2001). New aspects of Wnt signaling pathways in higher vertebrates. Curr. Opin. Genet. Dev. *11*, 547–553.
43. Elbi, C., Misteli, T., and Hager, G.L. (2002). Recruitment of dioxin receptor to active transcription sites. Mol. Biol. Cell *13*, 2001–2015.
44. Hughes, K., Nikolakaki, E., Plyte, S.E., Totty, N.F., and Woodgett, J.R. (1993). Modulation of the glycogen synthase kinase-3 family by tyrosine phosphorylation. EMBO J. *12*, 803–808.
45. Dajani, R., Fraser, E., Roe, S.M., Yeo, M., Good, V.M., Thompson, V., Dale, T.C., and Pearl, L.H. (2003). Structural basis for recruitment of glycogen synthase kinase 3beta to the axin-APC scaffold complex. EMBO J. *22*, 494–501.
46. Shaw, M., Cohen, P., and Alessi, D.R. (1997). Further evidence that the inhibition of glycogen synthase kinase-3beta by IGF-1 is mediated by PDK1/PKB-induced phosphorylation of Ser-9 and not by dephosphorylation of Tyr-216. FEBS Lett. *416*, 307–311.
47. Glinka, A., Wu, W., Onichtchouk, D., Blumenstock, C., and Niehrs, C. (1997). Head induction by simultaneous repression of Bmp and Wnt signalling in Xenopus. Nature *389*, 517–519.
48. Carnac, G., Kodjabachian, L., Gurdon, J.B., and Lemaire, P. (1996). The homeobox gene Siamois is a target of the Wnt dorsalisation pathway and triggers organiser activity in the absence of mesoderm. Development *122*, 3055–3065.
49. Kessler, D.S. (1997). Siamois is required for formation of Spemann's organizer. Proc. Natl. Acad. Sci. USA *94*, 13017–13022.
50. Zeng, L., Fagotto, F., Zhang, T., Hsu, W., Vasicek, T.J., Perry, W.L., 3rd, Lee, J.J., Tilghman, S.M., Gumbiner, B.M., and Costantini, F. (1997). The mouse Fused locus encodes Axin, an inhibitor of the Wnt signaling pathway that regulates embryonic axis formation. Cell *90*, 181–192.
51. Baker, J.C., Beddington, R.S., and Harland, R.M. (1999). Wnt signaling in Xenopus embryos inhibits bmp4 expression and activates neural development. Genes Dev. *13*, 3149–3159.
52. Bain, J., McLauchlan, H., Elliott, M., and Cohen, P. (2003). The specificities of protein kinase inhibitors: an update. Biochem. J. *371*, 199–204.
53. Williams, D.H., and Mitchell, T. (2002). Latest developments in crystallography and structure-based design of protein kinase inhibitors as drug candidates. Curr. Opin. Pharmacol. *2*, 567–573.
54. Leost, M., Schultz, C., Link, A., Wu, Y.-Z., Biernat, J., Mandelkow, E.-M., Bibb, J.A., Snyder, G.L., Greengard, P., Zaharevitz, D.W., et al. (2000). Paullones are potent inhibitors of glycogen synthase kinase-3beta and cyclin-dependent kinase 5/p25. Eur. J. Biochem. *267*, 5983–5994.
55. Dorronsoro, I., Castrob, A., and Martinez, A. (2002). Inhibitors of glycogen synthase kinase-3: future therapy for unmet medical needs? Expert Opin. Ther. Patents *12*, 1–10.
56. Bhat, R.V., and Budd, S.L. (2002). GSK3beta signalling: casting a wide net in Alzheimer's disease. Neurosignals *11*, 251–261.
57. Gozes, I. (2002). Tau as a drug target in Alzheimer's disease. J. Mol. Neurosci. *19*, 337–338.
58. Hoshi, M., Sato, M., Matsumoto, S., Noguchi, A., Yasutake, K., Yoshida, N., and Sato, K. (2003). Spherical aggregates of {beta}-amyloid (amylospheroid) show high neurotoxicity and activate tau protein kinase I/glycogen synthase kinase-3{beta}. Proc. Natl. Acad. Sci. USA *100*, 6370–6375.
59. De Ferrari, G.V., Chacon, M.A., Barria, M.I., Garrido, J.L., Godoy, J.A., Olivares, G., Reyes, A.E., Alvarez, A., Bronfman, M., and Inestrosa, N.C. (2003). Activation of Wnt signaling rescues neurodegeneration and behavioral impairments induced by beta-amyloid fibrils. Mol. Psychiatry *8*, 195–208.
60. Inestrosa, N., De Ferrari, G.V., Garrido, J.L., Alvarez, A., Olivares, G.H., Barria, M.I., Bronfman, M., and Chacon, M.A. (2002). Wnt signaling involvement in beta-amyloid-dependent neurodegeneration. Neurochem. Int. *41*, 341–344.
61. Phiel, C.J., Wilson, C.A., Lee, V.M., and Klein, P.S. (2003). GSK-3alpha regulates production of Alzheimer's disease amyloid-beta peptides. Nature *423*, 435–439.
62. Larner, A.J. (2002). Alzheimer's disease: targets for drug development. Mini Rev. Med. Chem. *2*, 1–9.
63. Noble, W., Olm, V., Takata, K., Casey, E., Mary, O., Meyerson, J., Gaynor, K., LaFrancois, J., Wang, L., Kondo, T., et al. (2003).

Cdk5 is a key factor in tau aggregation and tangle formation in vivo. Neuron *38*, 555–565.
64. Nieuwkoop, P.D., and Faber, J. (1967). Normal Table of *Xenopus laevis* (Amsterdam: North Holland Publishing Co.)
65. Wallace, A.C., Laskowski, R.A., and Thornton, J.M. (1995). LIGPLOT: a program to generate schematic diagrams of protein-ligand interactions. Protein Eng. *8*, 127–134.
66. DeLano, W.L. (2002). The PyMOL Molecular Graphics System. DeLano Scientific, San Carlos, CA.
67. Carson, M. (1991). Ribbons 2.0. J. Appl. Crystallogr. *24*, 958–961.
68. Bhat, R., Xue, Y., Berg, S., Hellberg, S., Ormo, M., Nilsson, Y., Radesater, A.C., Jerning, E., Markgren, P.O., Borgegard, T., et al. (2003). Structural insights and biological effects of glycogen synthase kinase 3-specific inhibitor AR-A014418. J. Biol. Chem. *278*, 45937–45945.
69. Bertrand, J.A., Thieffine, S., Vulpetti, A., Cristiani, C., Valsasina, B., Knapp, S., Kalisz, H.M., and Flocco, M. (2003). Structural characterization of the GSK-3β active site using selective and non-selective ATP-mimetic inhibitors. J. Mol. Biol. *333*, 393–407.

Note Added in Proof

While this work was in press, the crystal structure of GSK-3β in complex with several inhibitors was reported: the thiazole AR-A014418 [68] and staurosporine, **IO**, alsterpaullone, and the anilino-maleimide I-5 [69].